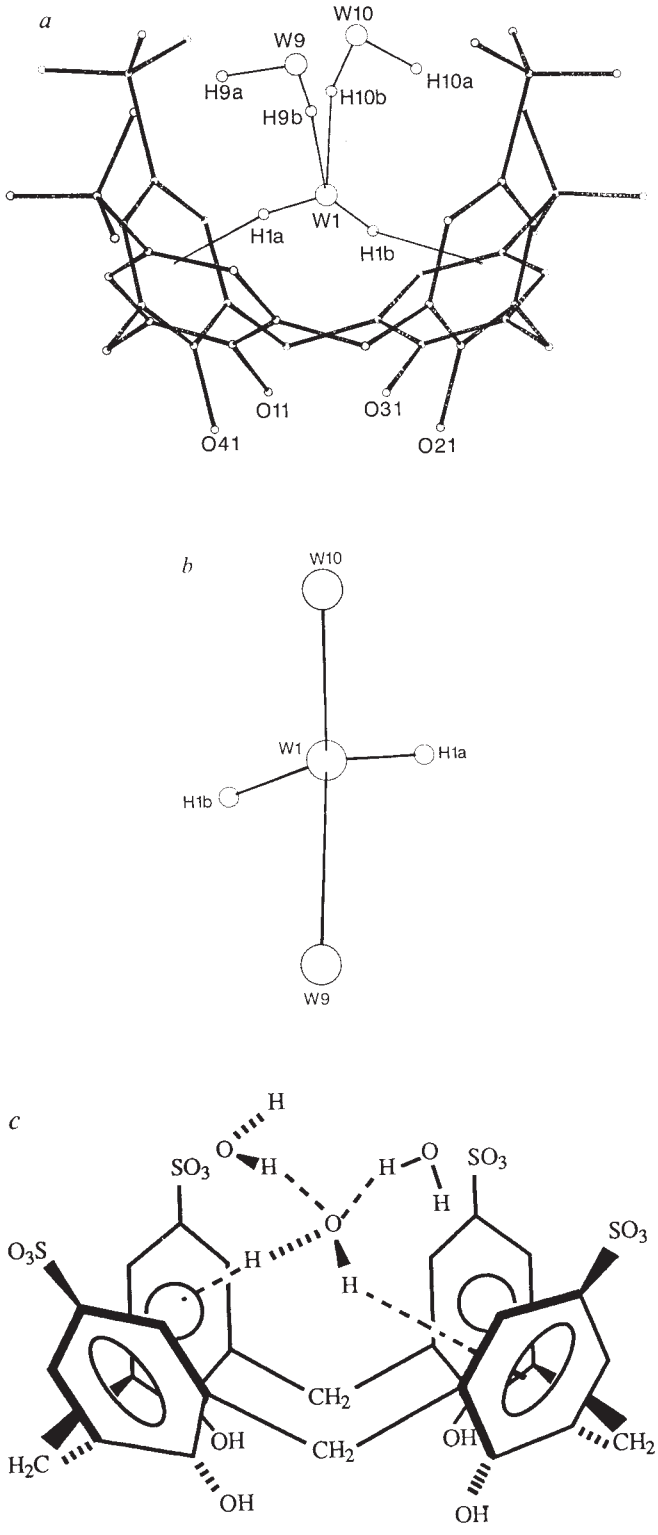

FIG. 1 *a*, The environment of the water molecule, W1, that exhibits π hydrogen bonding to two aromatic rings of the calix[4]arene. The calixarene carries a 4− charge conferred by the four sulphonate groups at the upper rim of the cavity. The phenolic oxygen atoms, O11, O21, O31 and O41, each possess a hydrogen atom. The rings involved in π hydrogen bonding with W1 are associated with O21 and O41. The two water molecules external to the cavity, W9 and W10, are involved in normal hydrogen bonding with W1. *b*, The imbedded water molecule W1 viewed from above W9 and W10 in the direction of the bottom of the calixarene cavity of *a*. The approximate tetrahedral coordination of W1 is emphasized. H1a and H1b are directed toward the π-electron density of the aromatic rings associated with O21 and O41 of *a*. *c*, Schematic illustration of the complete molecular complex.

in NaK_3[calix[4]arene sulphonate]·$9H_2O$, and there is one of 3.19 Å in [methylmorpholinocalix[4]arene]·3.5HCl·$9H_2O$. From this series of compounds it is clear that π-electron hydrogen bonding will be found in a wide range of crystal structures. This interaction must also be common in some biological environments. □

Received 30 August 1990; accepted 10 January 1991.

1. Burley, S. K. & Petsko, G. A. *Science* **229,** 23–35 (1985).
2. Tuchsen, E., Hayes, J. M., Ramaprasad, S., Copie, V. & Woodward, C. *Biochemistry* **26,** 5163–5172 (1987).
3. Gutsche, C. D. *Calixarenes* (Royal Society of Chemistry, Cambridge, 1989).
4. Vicens, J. & Bohmer, V. (eds) *Calixarenes* (Kluwer, Dordrecht, 1990).
5. Shinkai, S. *Pure appl. Chem.* **58,** 1523–1530 (1986).
6. Coleman, A. W. *et al. Angew. Chem. int. Ed. Engl.* **27,** 1361–1362 (1988).
7. Cheney, B. V., Schulz, M. W., Cheney, J. & Richards, W. G. *J. Am. chem. Soc.* **110,** 4195–4198 (1988).
8. Bredas, J. L. & Street, G. B. *J. Am. chem. Soc.* **110,** 7001–7005 (1988).
9. Karlstrom, G., Linse, P., Wallqvist, A. & Jonsson, B. *J. Am. chem. Soc.* **105,** 3777–3782 (1983).
10. Bredas, J. L. & Street, G. B. *J. chem. Phys.* **90,** 7291–7299 (1989).
11. Read, W. G., Campbell, E. J., Henderson, G. & Flygare, W. H. *J. Am. chem. Soc.* **103,** 7670–7672 (1981).
12. Read, W. G., Campbell, E. J. & Henderson, G. *J. chem. Phys.* **78,** 3501–3508 (1983).
13. Hamilton, W. C. & Ibers, J. A. *Hydrogen Bonding in Solids* 16 (Benjamin, New York, 1968).
14. Engdahl, A. & Nelander, B. *J. phys. Chem.* **89,** 2860–2864 (1985).
15. Wanna, J., Menapace, J. A. & Bernstein, E. R. *J. chem. Phys.* **85,** 1795–1805 (1986).
16. Jorgensen, W. L. & Severance, D. L. *J. Am. chem. Soc.* **112,** 4768–4774 (1990).

ACKNOWLEDGEMENTS. We thank the NSF for support.

Synthesis of inorganic nanophase materials in supramolecular protein cages

Fiona C. Meldrum, Vanessa J. Wade, Duncan L. Nimmo, Brigid R. Heywood & Stephen Mann*

School of Chemistry, University of Bath, Bath BA2 7AY, UK

THERE is currently great interest in the synthesis of inorganic materials of nanometre dimensions. The small size of these particles endows them with unusual structural and optical properties that may find application in catalysis and electro-optical devices. Such materials may also prove valuable as precursor phases to strong ceramics. Many approaches to the synthesis of these materials have focused on constraining the reaction environment through the use of surface-bound organic groups[1], polymers[2,3], porous glasses[4,5], zeolites[6], phospholipid vesicles[7,8] and reverse micelles[9]. Nanometre-sized particles may also be produced *in vivo* by microorganisms[10]. Here we describe a novel synthetic route based on the use of a supramolecular protein structure as a reaction cage in which to form inorganic phases. We show that the iron-storage protein ferritin can be used to generate nanometre-sized iron sulphide particles by *in situ* reaction of the iron oxide core of the native ferritin. Discrete nanoscale particles of manganese and uranium oxo-species can also be formed in the protein cavity. Our results highlight the potential of adapting natural biomineralization processes to problems in materials science, and suggest that the use of biological molecules and their synthetic analogues in mediating solid-state reactions constitutes a promising approach to nanophase engineering.

Ferritin is a robust iron-storage protein that can withstand high temperatures (85 °C) and pH (8.5–9) for limited periods without significant disruption of its quaternary structure of 24 polypeptide subunits. These subunits are assembled into a hollow sphere of 8–9 nm internal diameter[11] which contains an iron oxide core of structure similar to that of the mineral ferrihydrite ($5Fe_2O_3·9H_2O$). Hydrophilic and hydrophobic channels

* To whom correspondence should be addressed.

penetrate the protein shell and provide the means by which iron atoms can be accumulated within or removed from the molecules. *In vitro* reconstitution of iron (III) oxide cores can be readily achieved by room-temperature incubation of the intact empty protein (apoferritin) protein with Fe(II) solutions at moderate pH[12].

Figure 1 illustrates the general reaction schemes adopted in our work. Three approaches were undertaken: (*a*) *in situ* chemical reaction of native iron oxide cores with molecules and ions capable of penetrating into the internal cavity; (*b*) redox-driven reactions involving metal-ion uptake and deposition in apoferritin molecules; and (*c*) ion binding and hydrolytic polymerization of metal ions within apoferritin.

Following approach (*a*), iron sulphide particles were generated within ferritin by reaction of de-aerated solutions of the native protein (Cd-free, Boehringer Horse Spleen Ferritin) in 0.1 M AMPSO buffer (3-[(1,1-dimethyl-2-hydroxyethyl)amino]-2-hydroxypropanesulphonic acid), at pH 8.5 with H_2S. A black solution was formed within 20 s. A similar discolouration was observed for the reaction with Na_2S at pH 8.0, except that the formation of iron sulphide was significantly slower. In both cases, no bulk precipitation was observed, indicating that iron sulphide had been produced within the ferritin cavity by reaction of the native iron oxide cores. In comparison, analogous reactions involving synthetically prepared ferrihydrite suspensions resulted in an immediate black discolouration, followed within minutes by a black precipitate. Samples from the ferritin reaction were mounted onto carbon- and formvar-coated-nickel electron microscope grids and were studied immediately to minimize reoxidation reactions. Analysis was carried out by transmission electron microscopy (TEM), electron diffraction (ED) and energy-dispersive X-ray analysis (EDXA). Whereas the control experiments described above produced gel-like aggregates of amorphous iron sulphide, the protein samples showed discrete electron-dense cores (Fig. 2*a*) containing iron and sulphur (Fig. 2*b*). The particles formed in the H_2S preparation were irregular in shape, whereas those formed in the presence of Na_2S were generally spherical. The mean particle size and standard deviation were 6.8 nm and 1.2 nm, and 7.8 nm and 1.1 nm, for the H_2S and Na_2S samples respectively. Before reaction, the ferritin cores were spherical with a mean core diameter of 7.8 nm and standard deviation of 0.6 nm. This suggests that some iron may have been lost from the core on reaction with H_2S. EDXA analysis showed that the Fe/S ratio was close to unity for the H_2S product but was much greater for the Na_2S-derived particles, suggesting only partial reaction in the latter system. This is consistent with the electron diffraction patterns, which showed that some residual well crystallized ferrihydrite (six diffraction lines), characteristic of the original native ferritin core, was present in the iron sulphide cores formed by reaction with Na_2S. In contrast, the electron-dense cores prepared by addition of H_2S gave only three weak, broad ferrihydrite lines, demonstrating considerable loss in crystallinity on reaction. No diffraction lines corresponding to crystalline iron sulphides were observed.

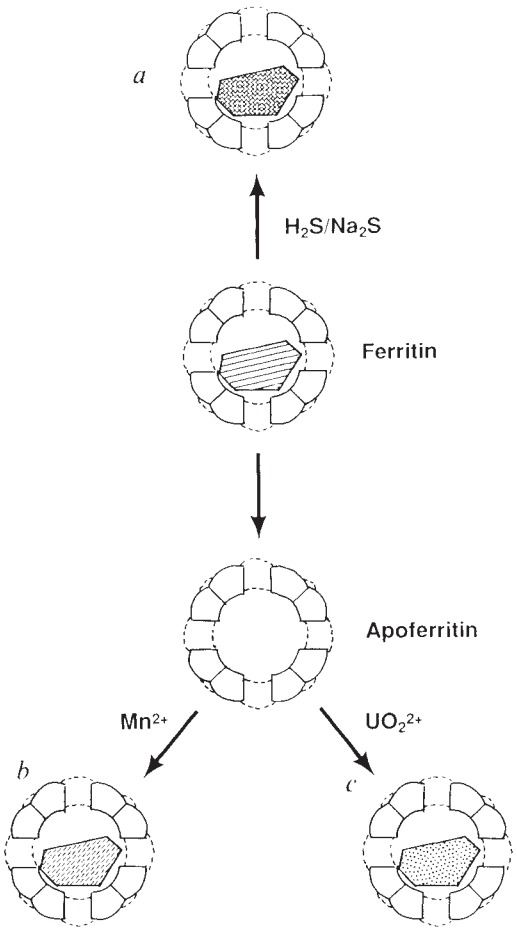

FIG. 1 Schematic representation of the use of ferritin in the synthesis of nanophase materials. *a*, Iron sulphide formation by *in situ* reaction of native iron oxide cores. *b*, Manganese oxide reconstitution by redox-driven reactions within apoferritin. *c*, Uranyl oxyhydroxide deposition by ion-binding and hydrolytic polymerization.

These results indicate that *in situ* transformation of ferritin iron oxide cores to discrete nanometre-sized iron sulphide particles can be readily achieved. Reaction with gaseous H_2S occurs more readily than with Na_2S, the latter giving mixed iron oxide and sulphide cores. This is probably due to more rapid penetration of the protein shell by the neutral H_2S molecules compared with charged HS^-/S^{2-} species.

Approach (*b*) was based on the reconstitution of apoferritin molecules with redox-active metal ions such as Mn(II). Apoferritin was prepared by repeated dialysis of ferritin solutions against a 0.5% solution of thioglycollic acid in 0.1 M sodium acetate buffer (pH 4.5), followed by dialysis against 0.15 M NaCl solution. Reconstitution of the protein to a theoretical value of 4,000 Mn ions per molecule was undertaken by combining buffered apoferritin solutions with $MnCl_2 \cdot 4H_2O$ solutions at pH values of 8.0–9.2. At pH 9, a fine-grained dark brown precipitate was observed in the protein-free control experiment after 4 h whereas the protein solution was a clear light brown colour, indicating specific deposition of manganeses oxides within the protein cavity. Experiments at lower pH were left for longer periods (up to two weeks). All reconstitutions showed evidence of some non-specific precipitation outside the protein cage.

Samples for TEM were either centrifuged and dialysed against 0.15 M NaCl or passed down a Sephadex G-25 chromatography column followed by reconcentration using an ultrafiltration cell. Discrete electron-dense particles of regular morphology, with mean size and standard deviation of 7.14 nm and 0.46 nm respectively, were imaged (Fig. 2*c*). EDXA spectra showed that the cores contained manganese (Fig. 2*d*). Electron diffraction patterns suggested that the manganese oxide cores were amorphous. By contrast, the non-specific product precipitated outside the protein cavities was identified as a mixture of the crystalline oxides groutite (α-MnOOH) and hausmannite (Mn_3O_4).

Bimetallic cores were prepared by similar experiments involving the successive addition of Fe(II) and Mn(II) solutions to apoferritin at pH 6.5 and pH 8.5 respectively. The resulting cores were discrete nanometre-size particles that contained both iron and manganese (data not shown). Electron diffraction patterns indicated that the Fe and Mn phases of individual cores were present as crystalline ferrihydrite and an amorphous oxide respectively. The influence of manganese on the magnetic properties of the ferrihydrite phase is currently under investigation.

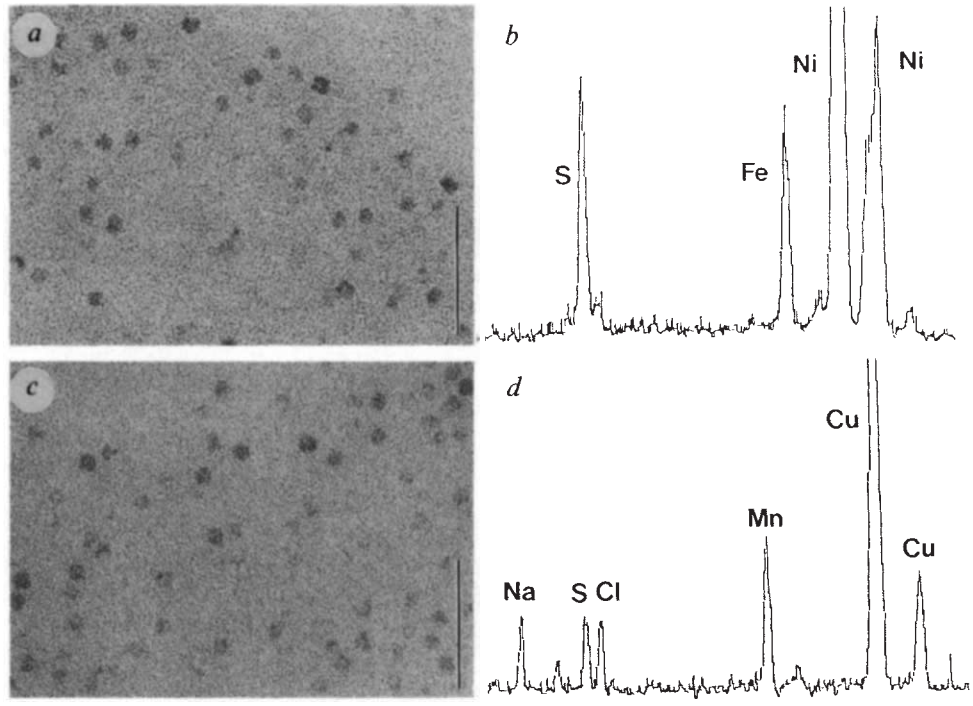

FIG. 2 TEM micrographs and corresponding EDXA spectra of iron sulphide cores (*a*, *b*) and manganese oxide cores (*c*, *d*) of ferritin. Scale bars in *a* and *c*, 50 nm. Ni and Cu peaks arise from the electron microscope grids; Na, Cl and S are background peaks from salt and buffer solutions.

These results indicate that apoferritin molecules can be reconstituted specifically with Mn(II) in a way similar to that commonly used for Fe(II)[12]. Mn(II) is known to bind to apoferritin with a stoichiometry of 8 ions per molecule[13], suggesting an initial binding site in the threefold channel. This site is presumably not involved in oxide deposition, which must involve migration of the manganese cations into the central cavity.

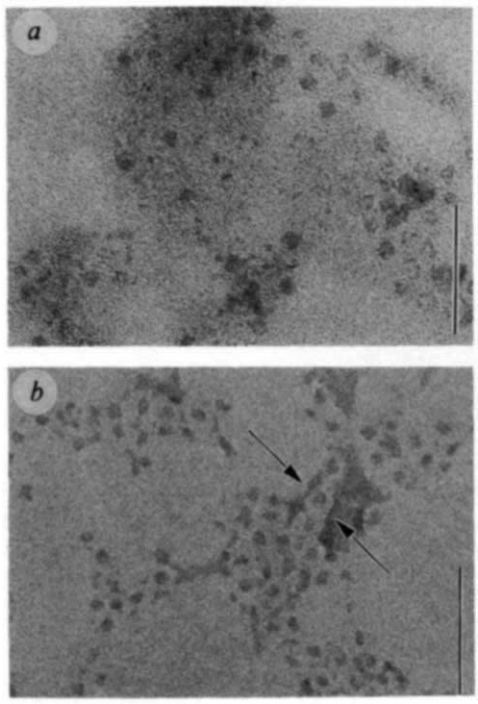

FIG. 3 *a*, TEM micrograph of apoferritin reconstituted with uranyl acetate, showing discrete cores of uranyl oxyhydroxide. *b*, As for *a*, but also showing evidence of negative staining of the external surface of the protein shell (arrows). Scale bars, 50 nm.

We have conducted similar experiments with other redox-active metal ions such as Ti(III), Co(II) and Cr(II). The results were less conclusive than those for the Mn(II) experiments. TEM analysis showed some evidence of reconstitution with Ti(III) and Cr(II), but the cores were very small and poorly defined. Effective reconstitution of the apoferritin molecules may depend on establishing the appropriate balance between many kinetic processes involving ion uptake, oxidation and polymerization, and factors such as ion concentrations, pH and redox potential may have to be carefully controlled in these reactions.

Finally, we have explored the possibility of using hydrolytic polymerization reactions as a basis for inorganic precipitation within the apoferritin cavity (Fig. 1*c*). The uranyl cation, UO_2^{2+}, is known to bind to apoferritin with a stoichiometry of 12 ions per molecule[14], possibly suggesting binding at the subunit dimer interface on the internal surface of the protein. A solution of $UO_2(O_2CCH_3)_2$ was added to apoferritin in 0.8 M TES (N-tris[hydroxymethyl]methyl-2-aminoethanesulphonic acid) at pH 8 in the dark to give a theoretical loading of 4,000 U atoms per apoferritin molecule. A yellow gel was formed after 24 h in both the protein and protein-free experiments. Analysis of the protein sample by TEM showed discrete electron-dense cores of mean diameter 6 nm (Fig. 3*a*), whereas similar analysis of the control experiment showed no discrete particles. Some cores showed associated staining of their surrounding protein coats by external UO_2^{2+} binding (Fig. 3*b*). No evidence of crystallinity in the polymerized uranyl oxyhydroxide was obtained.

Thus, supramolecular protein cages have the potential to act as constrained reaction environments in the synthesis of inorganic materials of nanometre dimension. The recent success in expressing human H-chain mutant ferritins[15] provides a possible route to the chemical tailoring of the inner surface of the protein cavity. We plan to investigate the use of such proteins in the oriented nucleation of spatially confined, crystallographically specific nanophase materials. □

Received 13 December 1990; accepted 17 January 1991.

1. Steigerwald, M. *et al. J. Am. chem. Soc.* **110**, 3046-3050 (1988).
2. Rossetti, R., Ellison, J. L., Gibson, J. M. & Brus, L. E. *J. chem. Phys.* **80**, 4464-4469 (1984).
3. Wang, Y., Liu, H. & Jiang, Y. *J. chem. Soc. chem. Commun.* 1878-1879 (1989).

4. Ekimov, A. I., Efros, Al. L. & Onushchenko, A. A. *Solid St. Commun.* **56,** 921–924 (1985).
5. Borrelli, N. F. *et al. J. appl. Phys.* **61,** 5399–5409 (1987).
6. Herron, N. *et al. J Am. chem. Soc.* **111,** 530–540 (1989).
7. Mann, S., Hannington, J. P. & Williams, R. J. P. *Nature* **324,** 565–567 (1986).
8. Heywood, B. R., Fendler, J. H. & Mann, S. *J. Colloid Interface Sci.* **138,** 295–298 (1990).
9. Inouye, K. *et al. J. phys. Chem.* **86,** 1465–1469 (1982).
10. Dameron, C. T. *et al. Nature* **338,** 596–597 (1989).
11. Ford, G. C. *et al. Phil. Trans. R. Soc. Lond.* B **304,** 551–565 (1984).
12. Macara, I. G., Hoy, T. G. & Harrison, P. M. *Biochem. J.* **126,** 151–162 (1972).
13. Wardeska, J. G., Viglione, B. & Chasteen, N. D. *J. biol. Chem.* **261,** 6677–6683 (1986).
14. Harrison, P. M. *et al.* in *Iron Transport in Microbes, Plants and Animals* (eds Winkelman, G., Van der Her, D. & Neilands, J. B.) 445–475 (VCH Publishers, New York, 1987).
15. Levi, L. *et al. J. biol. Chem.* **263,** 18086–18092 (1988).

Static strength and equation of state of rhenium at ultra-high pressures

Raymond Jeanloz, B. K. Godwal* & Charles Meade†

Department of Geology and Geophysics, University of California, Berkeley, California 94720, USA

YIELDING of materials is not understood well enough for detailed, quantitative predictions of strength to be possible, except by using semi-empirical models[1,2]. Studies of material strength at high pressures are therefore of fundamental as well as practical interest for determining the relationship between strength and other physical properties[3–6]. To this end, we have measured the shear stress (τ) supported by rhenium at pressures of up to 120 GPa, far higher than the pressures used in previous studies. Rhenium is of particular interest because it has the highest known bulk and shear moduli among metallic elements[7–9]. By using two independent methods of determining shear stress at room temperature, we find that rhenium is one of the strongest polycrystalline materials investigated so far, with shear stresses at high pressures reaching $\tau/\mu \approx 0.04(\pm 0.02)$ relative to the shear modulus μ. These values of τ/μ are nevertheless compatible with current theoretical expectations, indicating that the high strength of rhenium is not anomalous[1,2,6].

We compressed powdered rhenium (<5–10-μm grain size, 99.997% purity from Aesar, Johnson Matthey, Inc., Seabrook, New Hampshire) in a modified Mao–Bell type diamond cell[10]. The samples were confined by a spring-steel gasket between 1/4 carat diamonds with either 250-μm or 350-μm culets. Two runs were carried out with the sample contained in a small amount of pressure medium (≤50%(v/v) 4:1 methanol:ethanol) and a third run was conducted without any pressure medium; as a result, all of our experiments were conducted under conditions of varying, nonhydrostatic stress. Pressure distributions across the sample were determined by the ruby fluorescence method[11], and X-ray diffraction patterns were collected with monochromatic Mo Kα radiation from a rotating-anode source. The diffraction patterns are collected in an axial geometry, using film that is analysed in a manner described elsewhere[12]. The significance of the axial geometry, which is typical for such high-pressure measurements, is that the sample (or unit-cell) volume is determined from diffraction planes that all lie within <17° of the axis of force[11].

The pressure (P)–volume (V) measurements obtained at room temperature (Fig. 1*a*) can be analysed most critically by displaying them as Birch's[13] normalized pressure F as a function of the Eulerian strain measure f. Here,

$$F = P/[3f(1+2f)^{2.5}] = K_0[1 + a_1 f + a_2 f^2 + \ldots] \quad (1)$$

$$f = [(V/V_0)^{-2/3} - 1]/2 \quad (2)$$

with subscript zero indicating zero pressure. The second equality in equation (1) defines the finite-strain equation of state as a series expansion involving the zero-pressure bulk modulus, K_0, and its pressure derivatives: the first and second derivatives appear in the third- and fourth-order coefficients a_1 and a_2, respectively[13,14].

Figure 1*b* shows our data compared with a third-order equation of state (300-K isotherm) derived from ultrasonic measurements of K_0 and its first pressure derivative K_0' for Re (ref. 8). It is evident that all except possibly our highest-pressure data are biased relative to the ultrasonic equation of state, in that we obtain values of F that are too large at each strain f.

To confirm this result, we have reduced shock-wave measurements of the Hugoniot equation of state of rhenium by way of the Mie–Grüneisen formalism[14,15]. Recent calculations using the first-principles linearized muffin-tin-orbitals (LMTO) method[16] support the use of the Mie–Grüneisen approach for such an analysis (B.K.G. and R.J., unpublished work). In particular, the calculations show that the electronic structure of Re is essentially constant and the electronic contribution to the equation of state is negligible over the range of pressures considered here. In addition, we find that Re is expected to remain crystalline: according to the calculations it melts at much higher shock compressions than those of the data we analyse.

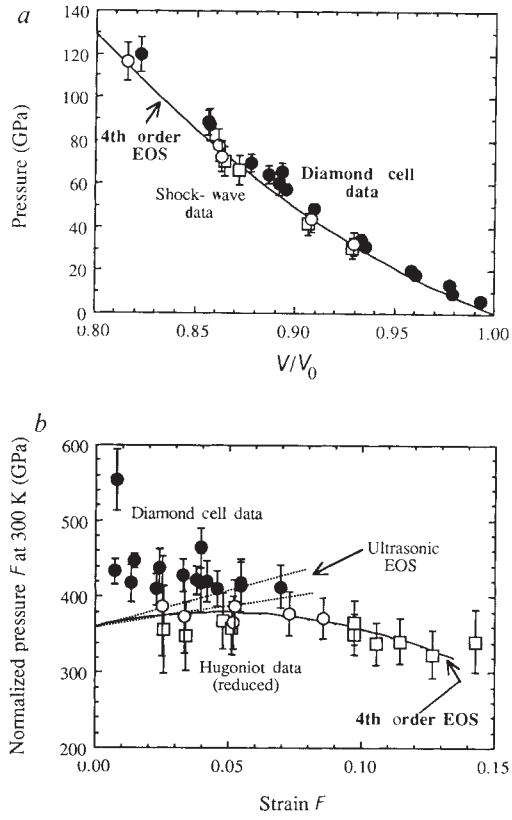

FIG. 1 Equation of state data for Re plotted in terms of volume compression as a function of pressure (*a*) and Birch's normalized pressure F as a function of the Eulerian strain parameter f (*b*) (equations (1) and (2)). The solid points are the present diamond-cell data collected at 300 K (one point at $f = 0.0023$, $F = 880 \pm 44$ GPa lies outside the range of plot *b*). The open symbols are the shock-wave data of ref. 23 reduced to a 300-K isotherm, with circles and squares corresponding to data collected from samples having initial porosities of 0.2% and 2.3%, respectively[14,15]. In reducing the Hugoniot data, the Grüneisen parameter was assumed to be given by $\gamma = \gamma_0(V/V_0)^q$, with $\gamma_0 = 2.65$ (±0.20) and $q = 1$ (±1) (refs 8, 14, 15, 24). The dashed lines in *b* indicate the envelope containing the isothermal third-order equation of state derived from the ultrasonic measurements and their uncertainties (ref. 8). The fourth-order fit to the ultrasonic and shock-wave measurements (reduced to the 300-K isotherm) is given by the solid line labelled '4th order EOS'.

* Permanent address: Neutron Physics Division, Bhabha Atomic Research Center, Trombay, Bombay 400085, Maharashtra, India.
† Present address: Geophysical Laboratory, Carnegie Institution of Washington, 5251 Broad Branch Road, Washington, DC 20015-1305, USA.